Journal of Power Sources 189 (2009) 972–981

Contents lists available at ScienceDirect

Journal of Power Sources

journal homepage: www.elsevier.com/locate/jpowsour

Synthesis and characterization of lanthanum silicate apatite by gel-casting route as electrolytes for solid oxide fuel cells

San Ping Jiang[a,*], Lan Zhang[a], Hong Quan He[a], Rong Keng Yap[a], Yan Xiang[b,*]

[a] School of Mechanical and Aerospace Engineering, Nanyang Technological University, Singapore 639798, Singapore
[b] School of Chemistry and Environment, Beihang University, Beijing 100191, PR China

ARTICLE INFO

Article history:
Received 12 November 2008
Received in revised form 15 December 2008
Accepted 15 December 2008
Available online 25 December 2008

Keywords:
Lanthanum silicate apatite
Electrolyte
Gel-casting technique
Solid oxide fuel cells
Conductivity

ABSTRACT

Lanthanum silicate oxyapatite, $La_{10}Si_6O_{27}$ is successfully synthesized by a water-based gel-casting technique. The effect of calcination and sintering temperatures on the conductivity is investigated in detail in the temperature range between 300 and 800 °C by the impedance spectroscopy. The highest oxygen ion conductivity is 1.50×10^{-3} S cm^{-1} at 500 °C and 3.46×10^{-2} S cm^{-1} at 800 °C for an apatite electrolyte sintered at 1650 °C, which is one order of magnitude higher than that synthesized by the conventional solid state reaction route under the same sintering conditions. The thermal expansion coefficient (TEC) of the as-synthesized apatite is 9.7×10^{-6} K^{-1}. A solid oxide fuel cell using $La_{10}Si_6O_{27}$ as an electrolyte shows an open circuit potential of 1.06 V and power output of 7.89 mW cm^{-2} at 800 °C. The results demonstrate the potential of the silicate oxyapatite materials synthesized by the gel-casting as an alternative electrolyte in solid oxide fuel cells.

1. Introduction

Solid oxide fuel cell (SOFC) operating at intermediate temperatures of 600–800 °C is attracting world attention owing to its promising benefits of the increased long-term stability, wide range of material selection and possibility of using low cost processing techniques. However, reducing the operating temperature of SOFC also increases the polarization losses associated with the electrode and electrolyte reactions. Thus, one of the major challenges in the development of intermediate temperature SOFCs is to develop a solid electrolyte material with a high conductivity to maintain the low ohmic loss during operation. A number of oxide ion conductors, such as the doped lanthanum gallate, doped ceria, yttria-stabilized zirconia (YSZ) have being developed for applications as the electrolytes in SOFCs [1–5]. Apatite-type oxides with a general formula $(La/M)_{10-x}(Si/GeO_4)_6O_{2\pm\delta}$ (M = Mg, Ca, Sr, Ba) are attracting considerable attention as a new class of electrolyte materials for SOFCs [6–11]. The structure of lanthanum silicate apatite consists of isolated Si/GeO_4 tetrahedral with La cations located in seven-coordinate and nine-coordinate cavity sites. Oxygen ions located in large conduction channels of the apatite structure suggest that this material should be appropriate for the electrolyte applications for SOFCs. In fact Nakayama et al. [12,13] reported that apatite structured oxides exhibit oxygen conductivities (4×10^{-3} S cm^{-1} at 500 °C) higher than of YSZ electrolyte at intermediate temperatures.

Lanthanum silicate apatites are usually prepared by solid state reaction (SSR) route using La_2O_3 and SiO_2 as raw materials and require a very high temperature (1575–1700 °C) and long dwelling time [6,7,12,14,15]. Tao and Irvine [16] studied the phase formation of $La_{10}Si_6O_{27}$ synthesized by a sol–gel method and found that the apatite phase can be formed at temperatures as low as 800 °C. However, the relative density of the sol–gel sample sintered at 1400 °C was less than 70% and prolonged sintering was not effective in the enhancing of the densification process. Hot-pressing at 1400 °C under 35 MPa resulted in a relative density of 92% but the conductivity was low, 2×10^{-4} S cm^{-1} at 700 °C, probably due to some contamination or the formation of secondary phase [11]. Doping with transition metals such as Fe can improve the sinterability of apatite ceramics prepared by a standard solid state reaction route, but the ionic conductivity is reduced significantly [14]. The presence of secondary phase, $La_2Si_2O_7$ in the binary phase diagram of the La_2O_3–SiO_2 system [17] indicates that it may be difficult to obtain a homogeneous mixture of the oxide precursors prepared by the conventional solid state reaction process. Celerier et al. [10] recently synthesized $La_{9.33}Si_6O_{26}$ ceramics by epoxide-driven sol–gel chemistry route. The relative density as high as 90–95% was obtained for the lanthanum silicate ambigel powder sintered at 1400 °C. By contrast, sintering the xerogel powder at 1400 °C only yielded a relative density of 70–80%. The drawback of the ambigel and xerogel process is the use of expensive chemicals and is time-consuming.

* Corresponding authors. Tel.: +65 6790 5010; fax: +65 6791 1859.
E-mail addresses: mspjiang@ntu.edu.sg (S.P. Jiang), xiangy@buaa.edu.cn (Y. Xiang).

0378-7753/$ – see front matter © 2008 Elsevier B.V. All rights reserved.
doi:10.1016/j.jpowsour.2008.12.064

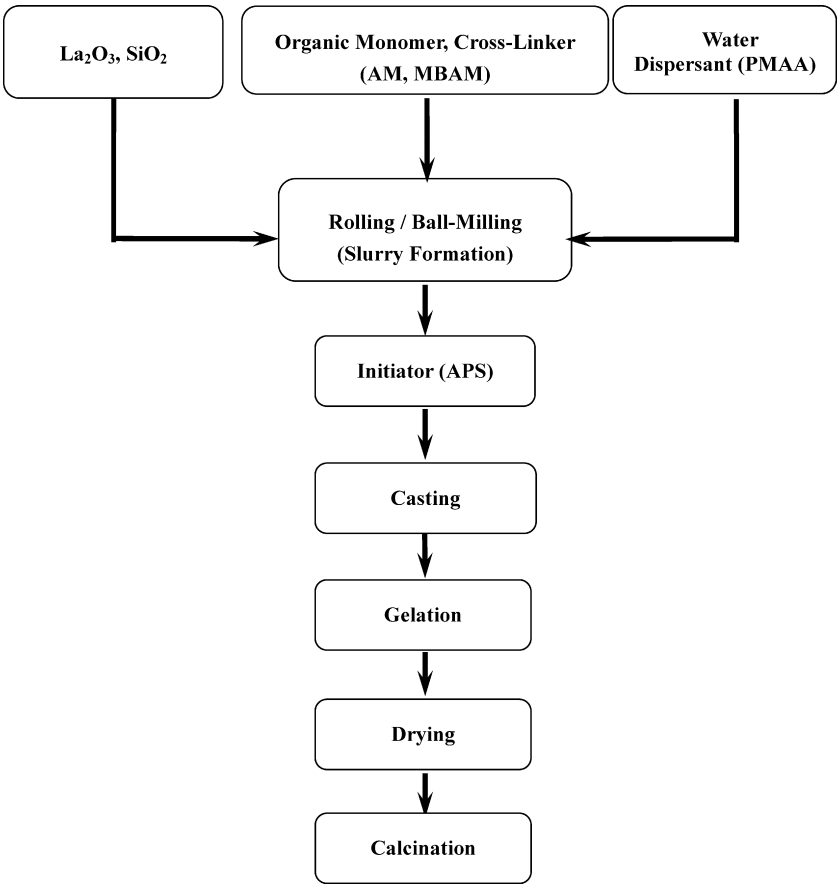

Fig. 1. Process flow chart for the synthesis of apatite powders by a water-based gel-casting technique.

We have recently applied water-based gel-casting technique to synthesize (La,Sr)(Cr,Mn)O_3 and (La,Sr)MnO_3 electrode powders for SOFC [18,19]. The electrode powder synthesized by the gel-casting technique shows a high electrocatalytic activity and the phase formation temperature is considerably lower than the powder synthesized by the conventional solid state reaction route. The reason is due to the uniformly distributed raw particles in a polymeric matrix formed during the gelation step. In this paper, $La_{10}Si_6O_{27}$ powders were synthesized by a water-based gel-casting technique. The effect of the powder calcination temperature on the phase formation and densification of apatite powders was studied by XRD and SEM. The results show that the apatite electrolyte prepared by the water-based gel-casting technique shows an improved sinterability and a much higher conductivity as compared to that prepared by the conventional solid state reaction method. Finally, a solid oxide fuel cell based on $La_{10}Si_6O_{27}$ electrolyte was fabricated and tested.

2. Experimental

2.1. Synthesis of $La_{10}Si_6O_{27}$ powders

High purity La_2O_3 and SiO_2 (all chemicals were from Sigma–Aldrich) were used without further treatment. The oxides were weighed, and mixed in a BMT-30D rolling machine with isopropanol solvent for 24 h, then dried in an oven at 80 °C. A solution of monomers consisted of acrylamide ($C_2H_3CONH_2$, AM, Sigma–Aldrich) and N,N′-methylene-bisacrylamide ($(C_2H_3CONH)_2CH_2$, MBAM, Sigma–Aldrich) was prepared in water and the ratio of AM to MBAM was 15 to 1. La_2O_3 and SiO_2 oxides were added in the premixed solution using ammonium poly-(methacrylate) ($(C_3H_5CO_2NH_4)_n$, PMAA, SD-03 Jiang Su, China) as the dispersant, followed by mixing in Planetary ball mill PM 400 for 10 min. Ammonium persulphate ($(NH_4)_2S_2O_8$, APS, Sigma–Aldrich, 2 wt% water solution) was added as the initiator. After stirred for several minutes, the slurry was poured into a container, and then heated in an oven at 80 °C to initiate the gelation. The gel was dried and calcined between 1000 and 1200 °C for 10 h in air, and the powders were dispersed in isopropanol and pulverized in a Planetary ball mill using YSZ balls as the milling medium. After dried, the powders were calcined at the same temperature for another 5 h in air. Fig. 1 shows the process flow chart for the synthesis of apatite powders by a water-based gel-casting technique (abbreviated as WGL). For the purpose of comparison, $La_{10}Si_6O_{27}$ powders were also prepared by a conventional solid state reaction method. La_2O_3 and SiO_2 with stoichiometric composition were mixed in isopropanol and ball milled for 24 h. The processes of calcinations, pulverization and calcinations for the SSR powders were the same as those for the WGL powders.

2.2. Characterization

The as-synthesized apatite powders were unaxially pressed into pellets and bars under a pressure of 150 MPa and sintered at 1550, 1600 and 1650 °C for 4 h in air. To reduce the shrinkage of the apatite powder, the powder was coarsened at temperatures 1200–1400 °C for 15 h in air. The sintered bars with ~9 mm in diameter and ~5 mm in thickness were used for thermal expansion coefficient (TEC) measurement using a TMA 2940 thermal expansion instrument from room temperature to 900 °C. Phase formation of the $La_{10}Si_6O_{27}$ powders synthesized by the WGL and SSR techniques was determined by X-ray diffraction (XRD, Philips MPD 1880) using Cu K_α radiation at room temperature.

The sintered pellets with ~9 mm in diameter and 1.5 mm in thickness were used for the electrochemical impedance analysis. Silver paste (Ferro Corporation USA) was painted onto both sides of the samples as the electrodes. For the impedance measurements, a Solartron 1260 frequency response analyzer was used over the frequency range of 1 MHz to 1 Hz. The samples were mounted in a compression jig with silver wire electrodes, and the measurements were made in a 50 °C interval in air between 300 and 800 °C. The microstructure of $La_{10}Si_6O_{27}$ pellets were examined by a scanning electron microscope (SEM, Leica S360).

2.3. Cell fabrication and testing

An apatite substrate with ~20 mm in diameter and ~1.2 mm in thickness was used for the cell performance testing. Platinum paste was painted onto both sides of the substrate as the working and counter electrodes. The reference electrode was painted as a ring at the edge on one side of the electrolyte substrate. The gap between the counter and ring reference electrodes was 4 mm. Pt mesh was used as the current collector for both the working and counter electrodes.

The cell performance was evaluated with a built-in-house test station. The cell was sealed between two alumina tubes with a ceramic paste (Ceramicabond 668, Aermco Products Inc., USA). During the test, hydrogen humidified at room temperature (3% H_2O/97% H_2) was fed to the anode side at a flow rate of 100 ml min^{-1}, while the cathode was exposed to air. Electrochemical measurements were performed using a Solartron 1260 frequency response analyzer in conjunction with a 1287 electrochemical interface. The overall cell impedance was measured in the frequency range of 100–0.01 Hz with signal amplitude of 10 mV at open circuit voltage over a temperature range of 700–900 °C.

3. Results and discussion

3.1. Phase formation and thermal expansion coefficient

The phase formation of apatite powders synthesized by WGL and SSR was investigated by XRD and the results are shown in Fig. 2. As evident from Fig. 2a, La_2O_3 phase is detected for the SSR $La_{10}Si_6O_{27}$ powders calcined at 1000 and 1100 °C. The formation of apatite phase occurs at ~1200 °C. La_2O_3 phase was also found for the WGL $La_{10}Si_6O_{27}$ powders calcined at 1000 °C. However, the complete phase formation of apatite phase for the WGL powder occurs at 1100 °C (Fig. 2b), which is 100 °C lower than that of the $La_{10}Si_6O_{27}$ powders synthesized by the conventional SSR method. The results indicate that $La_{10}Si_6O_{27}$ powders can be successfully synthesized by the WGL technique with a reduced phase formation temperature, similar to our previous results on $(La_{0.75}Sr_{0.25})_{1-x}(Cr_{0.5}Mn_{0.5})O_3$ (LSCM) and $(La_{0.8}Sr_{0.2})_{0.9}MnO_3$ (LSM) powders [18,19]. The reduction in the phase formation temperature is most likely due to the much better homogeneity and immobilization of the precursor particles by the cross-linked polymeric network formed during the cross-linking and gel formation steps [20].

The thermal expansion curves of as-synthesized apatite oxides are shown in Fig. 3. The dilatometric curves of $La_{10}Si_6O_{27}$ in air are approximately linear within the temperature range investigated. The average TEC calculated from the dilatometric curves is 9.7×10^{-6} K^{-1} for the WGL apatite, and 10.3×10^{-6} K^{-1} for the SSR apatite. The TEC value is close to other electrolyte materials, e.g., 10.0×10^{-6} K^{-1} for YSZ electrolyte [21], and 11.8×10^{-6} K^{-1} for $Ce_{0.8}Gd_{0.2}O_2$ [22].

3.2. Densification and microstructure

Densification and microstructure of the lanthanum silicate-based apatite oxides are critical for the ionic conductivity properties

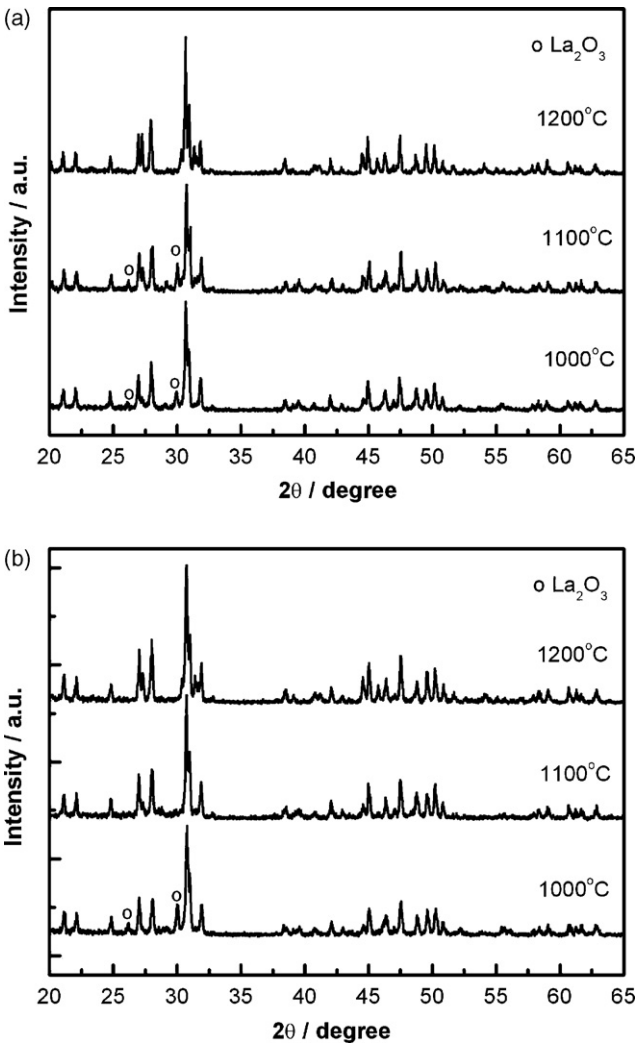

Fig. 2. XRD patterns of $La_{10}Si_6O_{27}$ powder synthesized by (a) solid state reaction, (b) water-based gel-casting techniques. The powder was calcined at different temperatures.

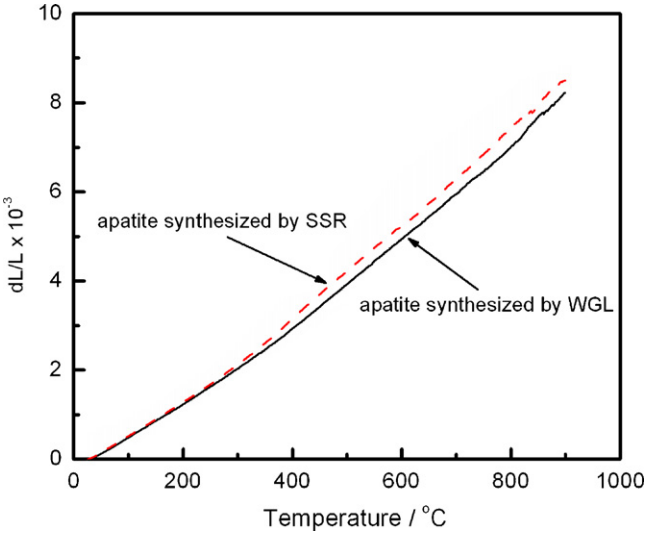

Fig. 3. Dilatometric curves of as-synthesized apatite prepared by solid state reaction and water-based gel-casting techniques.

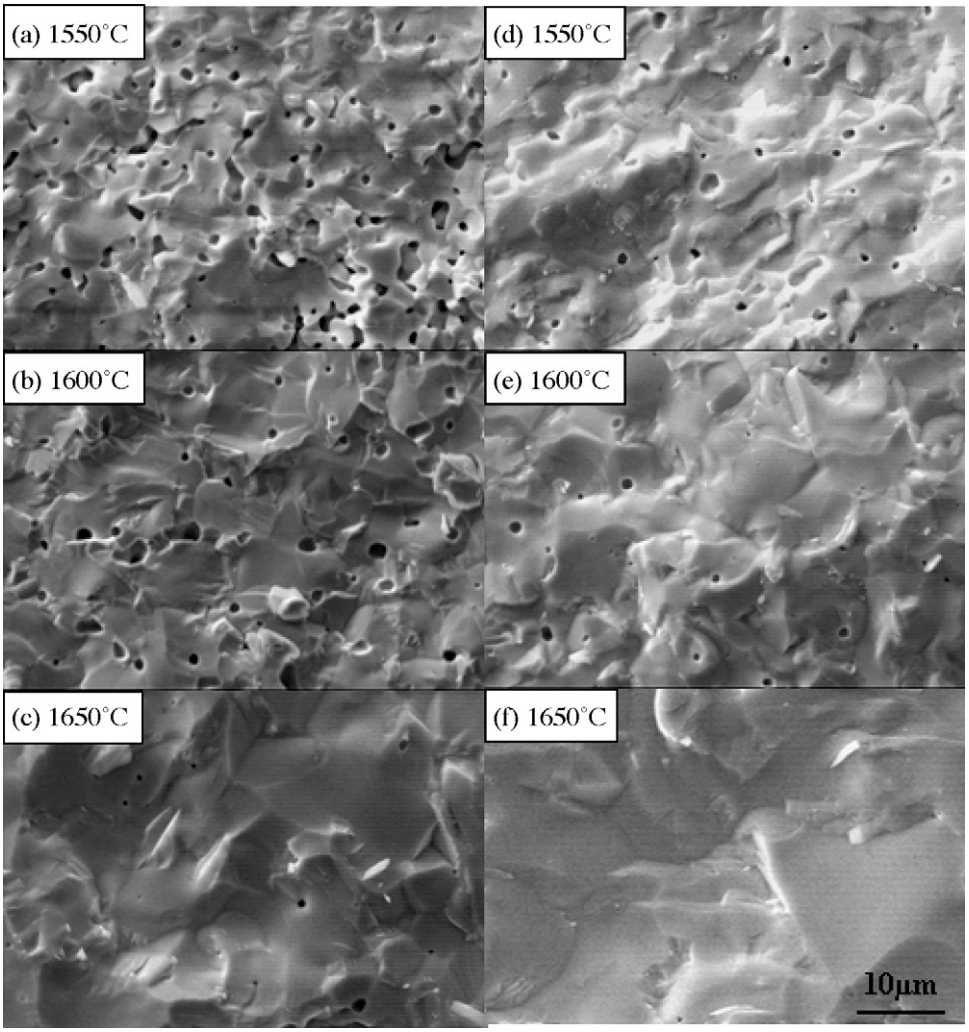

Fig. 4. SEM micrographs of fractured cross-sections of $La_{10}Si_6O_{27}$ samples synthesized by (a, b, c) SSR and (d, e, f) WGL method. The samples were prepared from the oxide powders calcinated at 1400 °C and sintered at 1550, 1600, and 1650 °C. The scale bar applies to all micrographs.

of the apatite electrolyte. Fig. 4 is the SEM micrographs of the fractured cross-sections of the $La_{10}Si_6O_{27}$ apatite disks prepared by the WGL and SSR methods and sintered at different temperatures. The powders were calcined at 1400 °C for 15 h in air. The porosity decreases with the increase in the sintering temperature. However, the number and size of pores of the SSR apatite samples are significantly higher than that of the WGL apatite samples sintered at 1550 and 1600 °C (Fig. 4a and b). When the sintering temperature increased to 1650 °C, the microstructure of both WGL and SSR apatite samples appears similar with substantially reduced porosity.

The difference in microstructure can be seen more clearly from the thermally etched samples. Fig. 5 shows the typical SEM micrographs of the thermally etched apatite samples sintered at different temperatures from the powders calcined at 1400 °C. There are some glassy or secondary phases formed on the apatite samples and the secondary phase appears to be accumulated along the grain boundaries. It can also be seen that there are more secondary phases for the SSR samples as compared to the WGL samples. For the samples sintered at 1650 °C, the apatite synthesized by both WGL and SSR is dense. However, for the SSR apatite samples, there is a glassy or secondary phase formed between the apatite grains (Fig. 5c). The average particle size is $4.93 \pm 2.8\,\mu m$, and $6.84 \pm 3.4\,\mu m$ for the WGL and SSR apatite samples. In addition to the increased densification, the WGL method also produces the apatite oxides with uniform grain size.

The significant differences in the microstructure of the apatite synthesized by WGL and SSR are clearly indicated by the bulk density of the $La_{10}Si_6O_{27}$ ceramic sintered at different temperatures, as showed in Fig. 6. As evident from Fig. 6a, the bulk density increases with the sintering temperature. The bulk density of WGL apatite sample is significantly higher than that of the SSR apatite samples sintered under the identical temperatures. At a sintering temperature of 1550 °C, the bulk density of the SSR apatite is $4.79\,g\,cm^{-3}$, which is significantly smaller than $5.30\,g\,cm^{-3}$ of the WGL apatite. However, as the sintering temperature increased to 1650 °C, the difference in the bulk density is reduced significantly, consistent with the SEM observation. This also indicates that the WGL technique is advantageous in enhancing the densification at low sintering temperatures as compared to the conventional SSR method. The densification of apatite oxides is also affected by the calcination temperature of the powder. However, the apatite oxide powder synthesized by WGL is much less sensitive to the pre-calcination temperature as compared to that synthesized by the SSR method (Fig. 6b). Table 1 summarizes the bulk and relative density of apatite oxides synthesized by the WGL and SSR sintered at different temperatures.

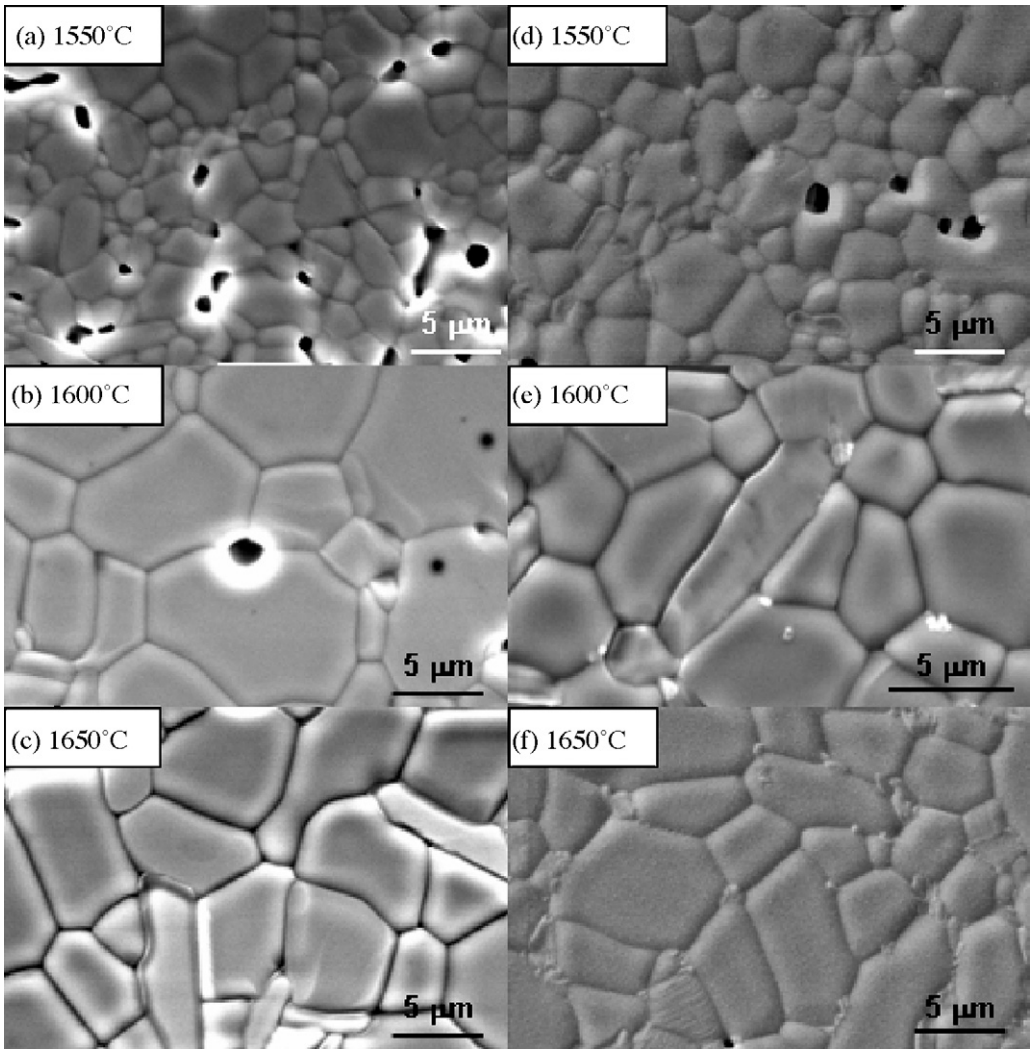

Fig. 5. SEM micrographs of the surface of thermally etched $La_{10}Si_6O_{27}$ samples synthesized by (a, b, c) SSR and (d, e, f) WGL method. The samples were prepared from the powder calcined at 1400 °C and sintered at 1550, 1600, and 1650 °C.

3.3. Impedance and conductivity properties

The conductivity of the lanthanum silicates prepared by the WGL and SSR methods was investigated by the electrochemical impedance spectroscopy in a temperature range of 300–800 °C. Fig. 7 is the complex impedance plots at 400 °C obtained for the WGL and SSR $La_{10}Si_6O_{27}$ sintered at different temperatures. The apatite powders were calcined at 1400 °C. The impedance response of the apatite oxides measured at 400 °C consists of two depressed semicircles at high and medium frequencies and a straight line at the low frequencies. The depressed semicircle at high frequencies arises from a small bulk contribution and the dominant semicircle at middle frequencies is due to the grain boundary response, similar to that observed on alumina-dispersed doped lanthanum gallates [23]. The declining line at the low frequencies belongs to the electrode process. The impedance arc at the middle frequencies of the apatite oxides synthesized by the SSR is substantially bigger than that synthesized by the WGL. This indicates the large grain boundary resistance of the SSR apatite oxides. The high grain boundary resistance is most likely due to the presence of the glassy or secondary phases at the grain boundaries (see Fig. 5). However, the separation of the bulk and grain boundary contributions from the impedance curves is difficult due to the substantial overlapping of the impedance arcs. This appears to be a general problem for the apatite systems [24,25]. Thus, the conductivities reported in this paper are the total conductivity.

The impedance responses of the apatite oxides also change significantly with the measuring temperature. Fig. 8 shows the

Table 1
Bulk density, relative density and average grain size of $La_{10}Si_6O_{27}$ apatite oxides synthesized by WGL and SSR methods as a function of sintering and calcination temperatures.

Calcination temperature (°C)	Sintering temperature (°C)	Bulk density/relative density ($g\,cm^{-3}$) (%)		Average grain size (μm)	
		WGL	SSR	WGL	SSR
1400	1550	5.30/94.27	4.79/85.25	2.80 ± 1.78	5.48 ± 4.22
1400	1600	5.33/94.79	5.11/91.02	4.82 ± 2.36	6.95 ± 5.408
1400	1650	5.39/95.95	5.29/94.13	4.94 ± 3.26	7.30 ± 4.583
1200	1550	5.31/94.45	5.30/94.31	n.a.	n.a.
1300	1550	5.30/94.40	5.27/93.74	n.a.	n.a.

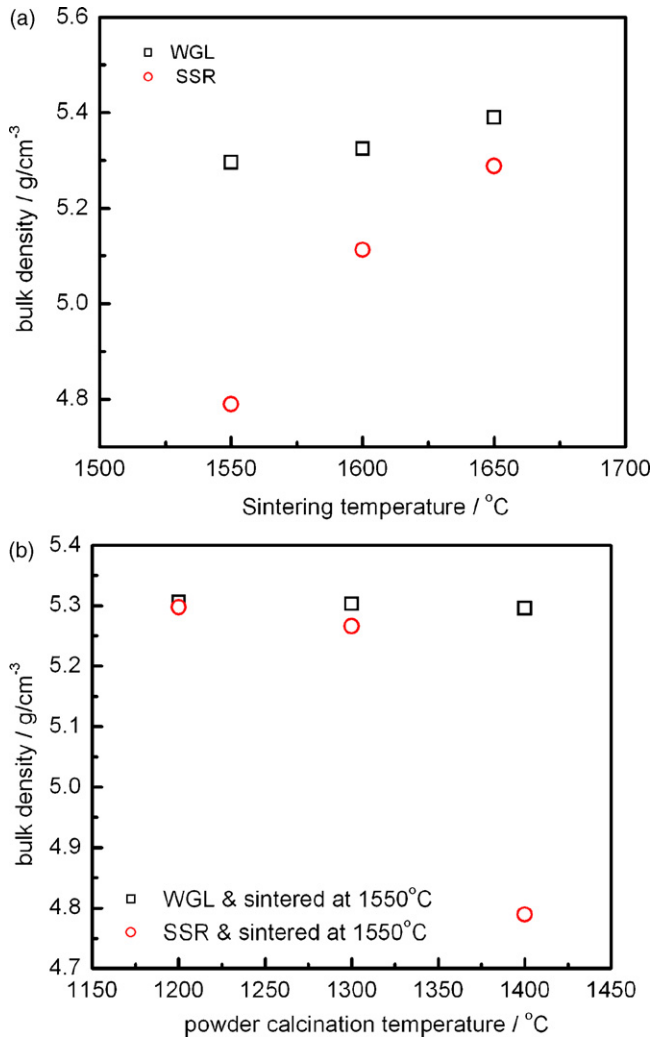

Fig. 6. Bulk density of $La_{10}Si_6O_{27}$ ceramic synthesized by WGL and SSR methods as a function of (a) sintering temperatures from the powders calcined at 1400 °C and (b) powder calcination temperatures with the final sintering temperature at 1550 °C.

impedance curves of a WGL $La_{10}Si_6O_{27}$ apatite sintered at 1650 °C, measured between 300 and 800 °C. Fig. 9 is the corresponding impedance curves of a SSR $La_{10}Si_6O_{27}$ apatite sintered at 1650 °C. The impedance curves at 400 and 600 °C exhibit two semicircles (see Fig. 8b and c). Above 650 °C, only one semicircle appears, indicating the dominance of the electrode process. In this case, the total resistance of the apatite sample was obtained from the high-frequency intercept. Table 2 lists the conductivity values of the WGL and SSR $La_{10}Si_6O_{27}$ ceramics as a function of the calcination and sintering temperatures, measured at different temperatures.

Fig. 10a shows the conductivity of the WGL and SSR $La_{10}Si_6O_{27}$ ceramics sintered at different temperatures, measured at 800 °C. The apatite powders were calcined at 1400 °C for 15 h in air. The conductivity of the WGL and SSR $La_{10}Si_6O_{27}$ ceramics increases with the sintering temperature and the conductivity of the WGL $La_{10}Si_6O_{27}$ is higher than that of the SSR $La_{10}Si_6O_{27}$ sintered at the same temperature. There is a significant increase in the conductivity for the WGL apatite samples sintered at 1650 °C while the increase in the conductivity for the SSR apatite is rather moderate. The significant increase in the conductivity for the WGL apatite sintered at 1650 °C as compared to that sintered at 1600 °C is, however, not clear at the moment. From the microstructure analysis (Fig. 5c), segregation and formation of glassy phases along the grain boundary are clearly observed. The existence of the secondary phases is detrimental to the ionic conductivity of the apatite samples. This again indicates the homogeneity of the precursors in the case of the WGL apatite is important to achieve the high ionic conductivity.

As seen in Fig. 10b, the conductivity of the WGL $La_{10}Si_6O_{27}$ ceramics is not affected by the powder calcination temperatures in the range studied for the apatite samples sintered at 1550 °C. In contrast, the powder calcination temperature has a significant effect on the conductivity of the SSR $La_{10}Si_6O_{27}$ ceramics. The densification and the relative density are critical for the conductivity of $La_{10}Si_6O_{27}$ electrolyte. For the SSR apatite samples, the bulk density is significantly related to the calcination temperature. As shown in Table 1, the bulk density is 4.79 g cm^{-3} for the SSR powder calcined at 1400 °C, significantly lower than 5.30 g cm^{-3} for the powder calcined at a lower temperature of 1200 °C. Thus, the significantly reduced conductivity for the SSR samples from the powder calcined at 1400 °C is due to the reduced relative density (Fig. 10b). On the other hand, the conductivity of the WGL samples is almost independent of the powder calcination temperature. This is due to the fact that precursors are immobilized in a polymeric matrix and the subsequent calcination has little effect on the distribution of the apatite powders.

3.4. Activation energy and electrochemical cell performance

The dependence of the total conductivity, σ of apatite electrolyte can be described by the Arrhenius equation,

$$\sigma = \frac{\sigma_0}{T} \exp\left(-\frac{E_a}{kT}\right) \quad (1)$$

where σ_0, E_a, k and T are the pre-exponential factor, activation energy, Boltzmann constant and absolute temperature. Fig. 11 shows the activation energy plots of the SSR and WGL apatite specimens as a function of the sintering and powder calcination temperatures. The activation energy for the ionic conductivity of WGL and SSR apatites is close, in the range of 75–87 kJ mol^{-1}. The best conductivity is obtained on the WGL apatite sintered at 1650 °C (Fig. 11a). At 500 °C, the conductivity is 1.50×10^{-3} S cm^{-1} which is

Table 2
Conductivity and activation energy of lanthanum silicate apatite synthesized by WGL and SSR techniques.

Samples	Calcination temperature (°C)	Sintering temperature (°C)	Conductivity (S cm^{-1})						E_a (KJ mol^{-1})
			300	400	500	600	700	800	
$La_{10}Si_6O_{27}$-WGL	1400	1650	1.39×10^{-5}	2.04×10^{-4}	1.50×10^{-3}	6.62×10^{-3}	1.81×10^{-2}	3.46×10^{-2}	87.85
$La_{10}Si_6O_{27}$-SSR	1400	1650	6.39×10^{-6}	6.56×10^{-5}	3.52×10^{-4}	1.20×10^{-3}	3.17×10^{-3}	6.22×10^{-3}	76.76
$La_{10}Si_6O_{27}$-WGL	1400	1600	6.88×10^{-6}	5.86×10^{-5}	3.15×10^{-4}	1.30×10^{-3}	3.53×10^{-3}	7.34×10^{-3}	79.51
$La_{10}Si_6O_{27}$-SSR	1400	1600	4.26×10^{-6}	3.93×10^{-5}	1.90×10^{-4}	6.56×10^{-4}	1.70×10^{-3}	3.51×10^{-3}	75.31
$La_{10}Si_6O_{27}$-WGL	1400	1550	7.78×10^{-6}	5.98×10^{-5}	2.70×10^{-4}	9.84×10^{-4}	2.69×10^{-3}	5.60×10^{-3}	74.49
$La_{10}Si_6O_{27}$-SSR	1400	1550	n.a.	2.15×10^{-5}	1.06×10^{-4}	3.85×10^{-4}	1.04×10^{-3}	2.27×10^{-3}	77.24
$La_{10}Si_6O_{27}$-WGL	1300	1550	4.10×10^{-6}	4.86×10^{-5}	2.71×10^{-4}	1.03×10^{-3}	2.77×10^{-3}	5.40×10^{-3}	80.26
$La_{10}Si_6O_{27}$-SSR	1300	1550	4.12×10^{-6}	3.37×10^{-5}	1.70×10^{-4}	6.0×10^{-4}	1.60×10^{-3}	3.31×10^{-3}	75.05
$La_{10}Si_6O_{27}$-WGL	1200	1550	6.49×10^{-6}	4.99×10^{-5}	2.65×10^{-4}	0.96×10^{-3}	2.56×10^{-3}	5.29×10^{-3}	76.19
$La_{10}Si_6O_{27}$-SSR	1200	1550	4.62×10^{-6}	3.60×10^{-5}	1.80×10^{-4}	0.62×10^{-3}	1.58×10^{-3}	3.27×10^{-3}	74.02

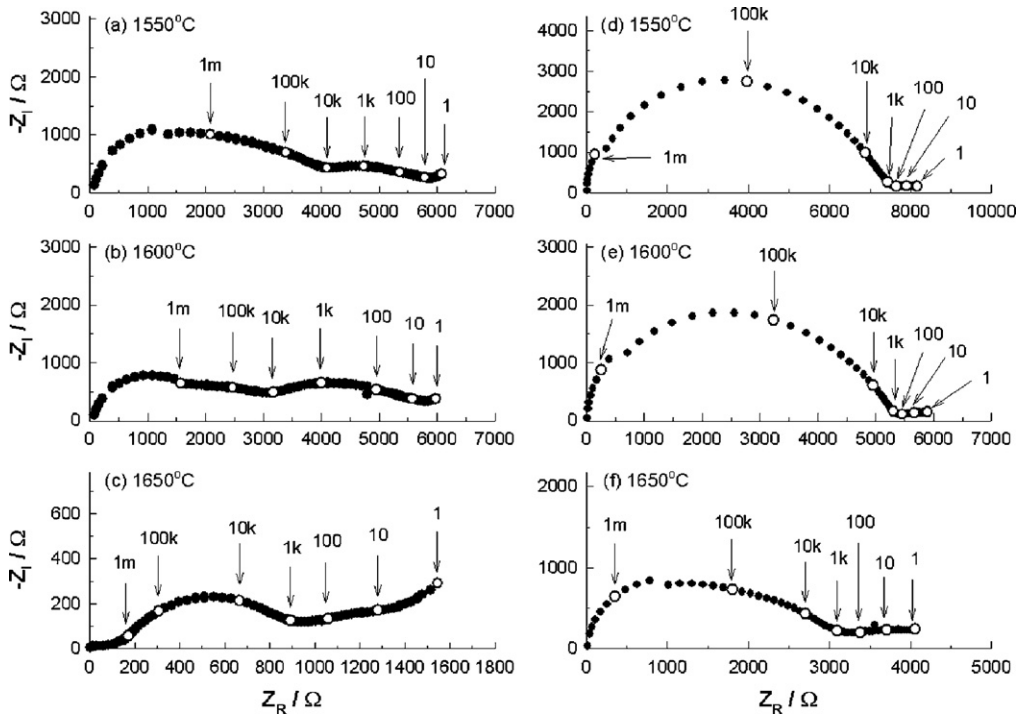

Fig. 7. Complex impedance plots obtained for (a, b, c) SSR and (d, e, f) WGL $La_{10}Si_6O_{27}$ sintered at different temperatures, measured at 400 °C. The apatite powders were calcined at 1400 °C. Numbers are frequencies in Hz.

significantly higher than 2.34×10^{-4} S cm^{-1} reported for the YSZ electrolyte at the same temperature [26]. The conductivity value of 1.50×10^{-3} S cm^{-1} at 500 °C on the WGL apatite is also very close to 4×10^{-3} S cm^{-1} for an apatite sintered at 1700 °C for 2 h reported by Nakayama et al. [12,13]. For the SSR apatite sintered at 1650 °C, the conductivity is 3.52×10^{-4} S cm^{-1} at 500 °C, almost one order of magnitude lower than that of the WGL apatite. For the apatite specimens sintered at 1550 °C, the effect of the pow-

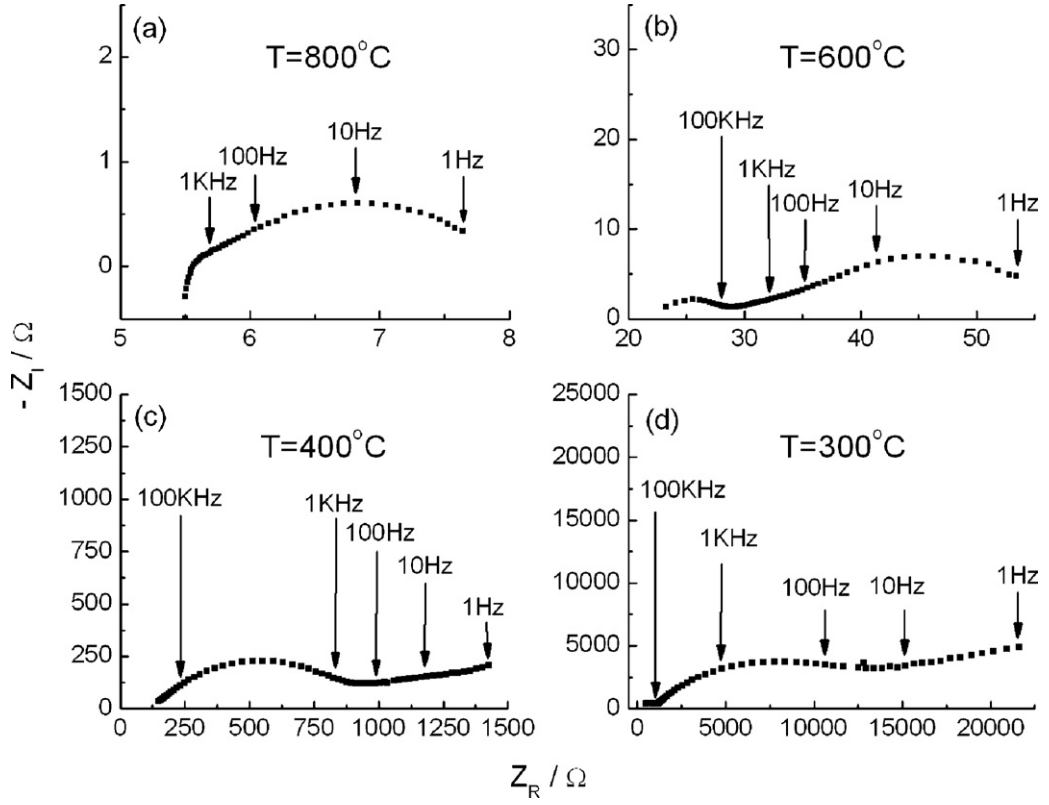

Fig. 8. Complex impedance curves measured at (a) 800 °C, (b) 600 °C, (c) 400 °C and (d) 300 °C for a WGL $La_{10}Si_6O_{27}$ sample sintered at 1650 °C for 4 h in air. Numbers are frequencies in Hz.

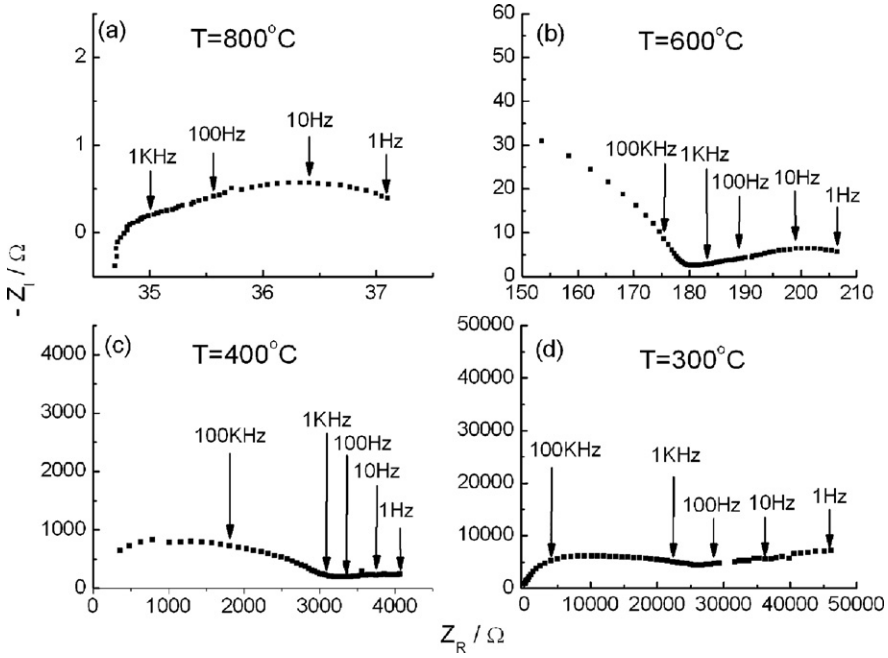

Fig. 9. Complex impedance curves measured at (a) 800 °C, (b) 600 °C, (c) 400 °C and (d) 300 °C for a SSR $La_{10}Si_6O_{27}$ sample sintered at 1650 °C for 4 h in air. Numbers are frequencies in Hz.

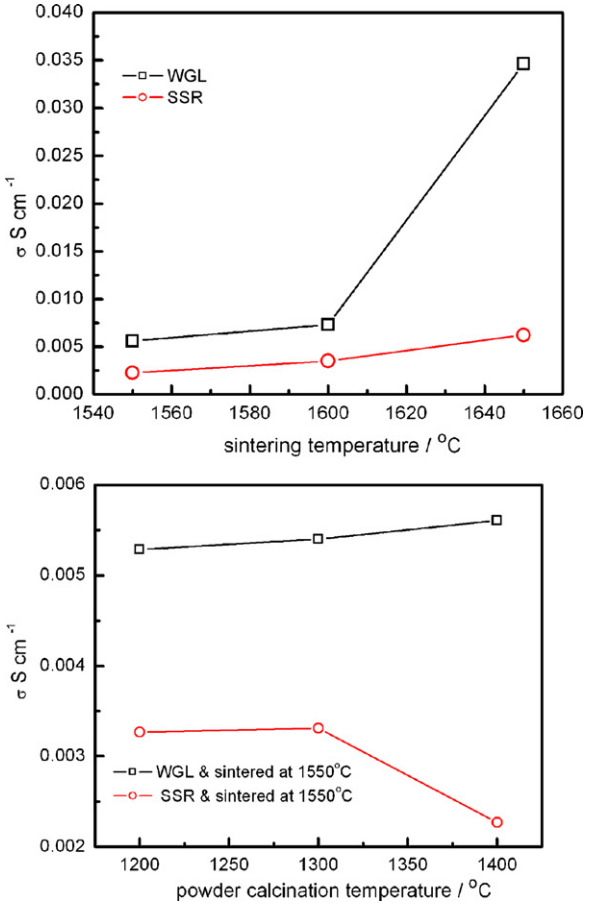

Fig. 10. Conductivity plots measured at 800 °C for (a) $La_{10}Si_6O_{27}$ samples prepared from the apatite powders calcined at 1400 °C and sintered at different temperatures, and (b) $La_{10}Si_6O_{27}$ samples prepared from the apatite powders calcinated at different temperature and sintered at 1550 °C.

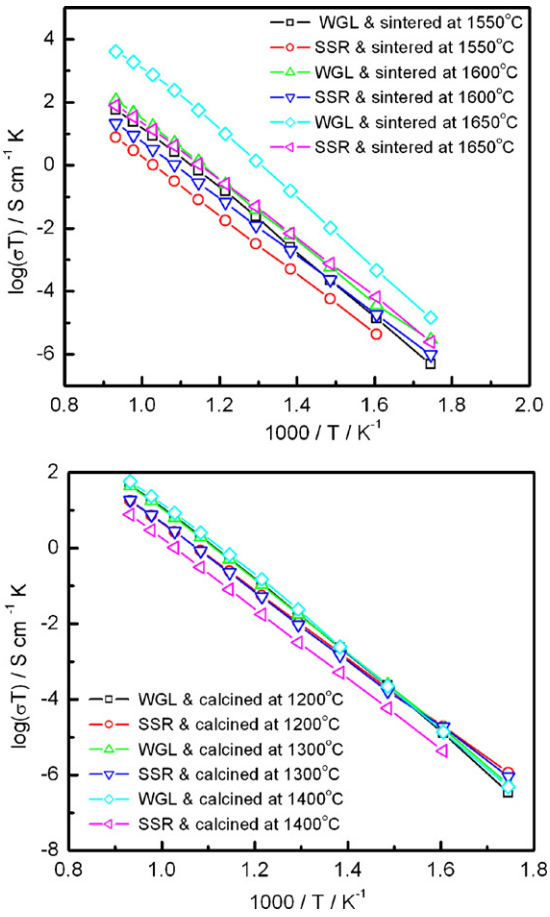

Fig. 11. Activation energy plots of SSR and WGL apatite specimens (a) prepared from the powder calcined at 1400 °C and sintered at different temperatures, and (b) prepared from the powder calcined at different temperatures and sintered at 1550 °C.

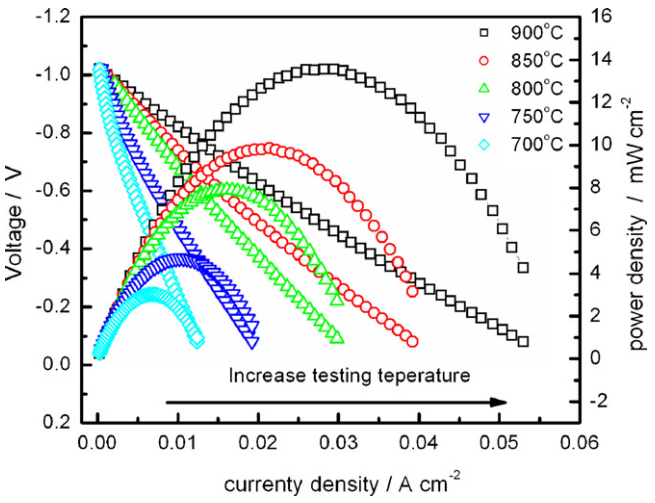

Fig. 12. Performance of a $La_{10}Si_6O_{27}$ electrolyte cell prepared by gel-casting technique with Pt anode and Pt cathode in H_2/air. The electrolyte was prepared from the apatite powder calcined at 1400 °C and sintered at 1600 °C.

der calcinations temperature on the conductivity is relatively small (Fig. 11b).

The conductivity (e.g., 3.46×10^{-2} S cm^{-1} at 800 °C) of WGL apatite sintered at 1650 °C in this study also compares favorably with the lanthanum silicate apatite with non-stoichiometric composition. Sansom et al. [7,27] reported a conductivity of 2×10^{-3} S cm^{-1} at 800 °C on $La_{9.33}Si_6O_{26}$ sintered at 1600 °C and 2.02×10^{-3} S cm^{-1} at 800 °C on $La_{9.33}Si_6O_{26}$ sintered at 1700 °C.

A cell consisted of a 1.2-mm-thick WGL $La_{10}Si_6O_{27}$ apatite electrolyte and Pt anode and Pt cathode was tested in H_2/air at different temperatures and the performance is shown in Fig. 12. The open circuit potential is 1.06 V at 900 °C, close to the theoretical value. This indicates the pure oxygen ionic conductivity of the apatite electrolyte with negligible electronic conductivity, consistent with the high ionic transfer numbers reported for the lanthanum silicate apatite oxides [28]. The cell performance is very poor and the maximum power density generated by the cell is 13.54, 7.89, 3.02 mW cm^{-2} at 900, 800, and 700 °C, respectively. Fig. 13 shows the corresponding impedance spectra of the cell measured at different temperatures under open circuit conditions. The impedance responses of the cell are characterized by a very larger

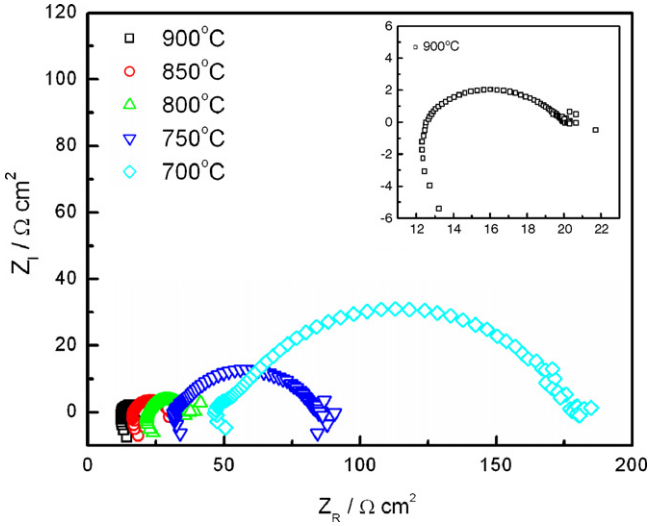

Fig. 13. Impedance spectra of the apatite electrolyte cell measured at different temperatures under open circuit in H_2/air.

and depressed arc. The overall electrode polarization resistance (or the area specific resistance, ASR) of the cell was obtained from the differences of the high- and low-frequency intercepts and the cell ohmic resistance was obtained from the high-frequency intercept. The ASR is 7.7 and 17.1 Ω cm^2 at 900 and 800 °C, respectively. The high ASR is clearly due to the poor electrocatalytic activity of Pt for both the hydrogen oxidation and oxygen reduction reactions of SOFCs [29–31].

The cell ohmic resistance is also very high. For example, at 800 °C, the cell ohmic resistance is 22.02 Ω cm^2. This is substantially higher than the theoretical electrolyte resistance value of 3.47 Ω cm^2 based on the electrolyte thickness (i.e., 1.2 mm) and the measured conductivity at 800 °C for the WGL apatite. The significantly high cell resistance with apatite electrolyte was also reported by Yoshioka and Tanase [32]. On a cell with a 0.493-mm-thick magnesium doped lanthanum silicate apatite electrolyte and Pt anode and Pt cathode, the measured cell resistance is 157 Ω cm at 805 °C, five times larger than 33 Ω cm calculated from the electrolyte. The reasons for the significantly higher cell resistance are not clear at this stage. One possible reason could be related to the porous Pt electrodes. Porous electrode has low contacts between the electrode and electrolyte interface, which can significantly increase the constriction effect and leads to the increase in the cell ohmic resistance [33]. The high ASR and high cell ohmic resistance indicate that much more work is needed before the apatite-based electrolyte could be applied to the intermediate temperature SOFCs.

4. Conclusions

Lanthanum silicate oxides were synthesized by a water-based gel-casting technique and a conventional solid state reaction method using oxide precursors for the potential applications as oxygen conducting electrolyte in solid oxide fuel cells. The XRD analysis confirmed the phase formation of the lanthanum silicate apatite structure at 1100 °C for the gel-casting apatite ceramics, which is 100 °C lower than that of the apatite synthesized by the conventional solid state reaction method. The best conductivity of the WGL apatite sintered at 1650 °C is 3.46×10^{-2} S cm^{-1} at 800 °C, which is significantly higher than 6.22×10^{-3} S cm^{-1} for the SSR apatite. The results in the present study demonstrate that the water-based gel-casting technique is an effective method to synthesize the lanthanum silicate powders with reduced sintering and phase formation temperatures. The average TEC of as-synthesized apatite by water-based gel-casting was $\sim 9.7 \times 10^{-6}$, close to those common used SOFC electrolyte materials. The performance of the cell with a 1.2-mm-thick $La_{10}Si_6O_{27}$ electrolyte and Pt anode and Pt cathode is very poor, indicating that much more work is needed before the apatite-based electrolyte could be applied to the intermediate temperature SOFCs.

Acknowledgement

The work is supported by Academic Research Fund AcRF tier 2 (ARC 2/08), Ministry of Education, Singapore, and by the National Nature Science Foundation of China (20773008) and National High-tech R&D 863 program (2007AA05Z146.

References

[1] H. Jena, B. Rambabu, Materials Chemistry and Physics 101 (2007) 20–29.
[2] W.N. Zhai, C. Ye, F. Xia, J.Z. Xiao, L. Dai, Y.F. Yang, Y.Q. Wang, Journal of Power Sources 162 (2006) 146–150.
[3] C.D. Zuo, S.W. Zha, M.L. Liu, M. Hatano, M. Uchiyama, Advanced Materials 18 (2006) 3318.
[4] P. Egger, G.D. Soraru, S. Dire, Journal of the European Ceramic Society 24 (2004) 1371–1374.

[5] X.Q. Sha, Z. Lu, X.Q. Huang, J.P. Miao, L. Jia, X.S. Xin, W.H. Su, Journal of Alloys and Compounds 424 (2006) 315–321.
[6] A. Vincent, S.B. Savignat, F. Gervais, Journal of the European Ceramic Society 27 (2007) 1187–1192.
[7] J.E.H. Sansom, A. Najib, P.R. Slater, Solid State Ionics 175 (2004) 353–355.
[8] L. Leon-Reina, E.R. Losilla, M. Martinez-Lara, S. Bruque, M.A.G. Aranda, Journal of Materials Chemistry 14 (2004) 1142–1149.
[9] P.R. Slater, J.E.H. Sansom, J.R. Tolchard, Chemical Record 4 (2004) 373–384.
[10] S. Celerier, C. Laberty-Robert, J.W. Long, K.A. Pettigrew, R.M. Stroud, D.R. Rolison, F. Ansart, P. Stevens, Advanced Materials 18 (2006) 615.
[11] P.J. Panteix, I. Julien, D. Bernache-Assollant, P. Abelard, Materials Chemistry and Physics 95 (2005) 313–320.
[12] S. Nakayama, M. Sakamoto, Journal of the European Ceramic Society 18 (1998) 1413–1418.
[13] S. Nakayama, T. Kageyama, H. Aono, Y. Sadaoka, Journal of Materials Chemistry 5 (1995) 1801–1805.
[14] A.L. Shaula, V.V. Kharton, J.C. Waerenborgh, D.R. Rojas, F.M.B. Marques, Journal of the European Ceramic Society 25 (2005) 2583–2586.
[15] J.E.H. Sansom, P.R. Slater, Solid State Ionics 167 (2004) 23–27.
[16] S.W. Tao, J.T.S. Irvine, Materials Research Bulletin 36 (2001) 1245–1258.
[17] N.A. Toropov, I.A. Bondar, Y. Galakhov, Trans. Int. Ceram. Eighth Congr. 1962, Coprehagen, Denmark: International Ceramic Congress, Paris, France, (1962) pp. 85–103.
[18] S.P. Jiang, L. Zhang, Y. Zhang, Journal of Materials Chemistry 17 (2007) 2627–2635.
[19] L. Zhang, Y.J. Zhang, Y.D. Zhen, S.P. Jiang, Journal of the American Ceramic Society 90 (2007) 1406–1411.
[20] C.S. Cheng, L. Zhang, Y.J. Zhang, S.P. Jiang, Solid State Ionics 179 (2008) 282–289.
[21] L.J. Gauckler, D. Beckel, B.E. Buergler, E. Jud, U.R. Muecke, M. Prestat, J.L.M. Rupp, J. Richter, Chimia 58 (2004) 837–850.
[22] H. Yokokawa, N. Sakai, T. Horita, K. Yamaji, M.E. Brito, Materials Research Society Bulletin 30 (2005) 591–595.
[23] I. Yasuda, Y. Matsuzaki, T. Yamakawa, T. Koyama, Solid State Ionics 135 (2000) 381–388.
[24] J.E.H. Sansom, D. Richings, P.R. Slater, Solid State Ionics 139 (2001) 205–210.
[25] J. McFarlane, S. Barth, M. Swaffer, J.E.H. Sansom, P.R. Slater, Ionics 8 (2002) 149.
[26] L.G. Cong, T.M. He, Y.A. Ji, P.F. Guan, Y.L. Huang, W.H. Su, Journal of Alloys and Compounds 348 (2003) 325–331.
[27] J.E.H. Sansom, J.R. Tolchard, P.R. Slater, M.S. Islam, Solid State Ionics 167 (2004) 17–22.
[28] A.L. Shaula, V.V. Kharton, F.M.B. Marques, Journal of Solid State Chemistry 178 (2005) 2050–2061.
[29] S.P. Jiang, Journal of Applied Electrochemistry 31 (2001) 181–192.
[30] T. Jacobsen, K.V. Hansen, E. Skou, Journal of the Electrochemical Society 152 (2005) A2203–A2206.
[31] S.P. Jiang, S.P.S. Badwal, Journal of the Electrochemical Society 144 (1997) 3777–3784.
[32] H. Yoshioka, S. Tanase, Solid State Ionics 176 (2005) 2395–2398.
[33] S.P. Jiang, J.G. Love, L. Apateanu, Solid State Ionics 160 (2003) 15–26.